Modeling and Simulation of the Fluid-Structure Interactions in Passively-Pitching Flapping Wings of Flying Microrobots

Longlong Chang and Néstor O. Pérez-Arancibia

***Abstract*— We present a study of the dynamics of passive wing-pitching in flapping-wing hovering flight, employing an integrated simulation approach. Here, the motion of a perfectly rigid wing is described using the Euler-Lagrange equation in Kane's formulation, in which the passive rotating mechanism (flexure hinge) is modeled as a single-axis elastic beam and the total aerodynamic moment is computed by numerically solving the three-dimensional Navier-Stokes equations for the low Reynolds number case using an overset grid method. The proposed approach leads to the formulation of a *fluid-structure interaction* (FSI) problem, which is solved using an alternating time-marching procedure. The presented integrated simulation approach is validated using experimental data available in the technical literature and the effect of different wing-planform shapes on the resulting aerodynamic efficiency is discussed.**

I. Introduction

The development of micro-mechanisms based on the notion of passive wing-pitching made possible the design and fabrication of insect-scale flapping-wing aerial microrobots. For example, in [1], the robot's wings are flapped actively, but the pitching motion is generated passively by allowing the wings to rotate about flexure hinges. As the wings' instantaneous angles of attack are mainly determined by the pitching angles, the wings' rotational motions directly affect the aerodynamic efficiency of the entire aerial robot. In the passive pitching case, the pitching rotation of a flapping wing is not prescribed and it results from the influence of inertial forces acting on the wing and the interaction of the airfoil with the surrounding air, as the wing is flapped and the flexure hinge flexes, defining a fluid-structure interaction problem. Passive pitching mechanisms have been studied experimentally and using quasi-steady blade element analyses [2]. However, in order to systematically study novel aerodynamic designs and robust control methods, passive wing-pitching mechanisms need to be investigated employing more sophisticated descriptions of the fluid-structure interaction phenomena that emerge in this case.

Considering that numerical Navier-Stokes solvers are widely used in research relating to the aerodynamics and flight mechanics of wings with fully prescribed flapping and pitching motions [3], we propose a simulation scheme that combines the solution of the wing's equations of motion with the outputs from the *three-dimensional* (3-D) aerodynamic solver employed to compute numerical solutions to the Navier-Stokes equations. This approach leads to the formulation of an integrated computational simulation framework, which can be extended to the study of the dynamics of an entire microrobot composed of flexure-hinge mechanisms.

II. Dynamical Modeling

We consider the dynamics of generic insect-scale flapping-wing microrobots of the kind depicted in Fig. 1, assuming the same basic aerodynamic and robotic designs to those of the prototypes in [1]. Typically, a robot of the kind considered here is composed of an airframe, a pair of power actuators, a pair of mechanical transmissions and a pair of flexure hinges that connect the wings through the transmissions to the power actuators. The microrobotic mechanisms employed in the construction of microrobots propelled by passively-pitching flapping wings are composed of rigid bars connected by rectangular flexure hinges, which can be modeled as single-axis elastic beams with stiffness k_h [2], as shown in Fig. 1-(b). Employing this simplified hinge model and assuming a perfectly rigid thin airfoil, the motion of a passively-pitching flapping wing can be described, using the Euler-Lagrange method in Kane's formulation, as

$$\frac{\mathrm{d}}{\mathrm{d}t}\left(\frac{\partial L}{\partial \dot{q}}\right) - \frac{\partial L}{\partial q} = \mathbf{F}_\mathrm{c}\cdot\frac{\partial \mathbf{v}_\mathrm{c}}{\partial \dot{q}} + \mathbf{M}_\mathrm{c}\cdot\frac{\partial \boldsymbol{\omega}}{\partial \dot{q}}, \qquad (1)$$

where L is the Lagrangian of the system, q is a generalized coordinate, $\mathbf{F}_\mathrm{c}$ and $\mathbf{M}_\mathrm{c}$ are, respectively, the non-conservative total force and total moment acting on the wing's center of mass, $\mathbf{v}_\mathrm{c}$ is the translational velocity of the wing's center of mass and $\boldsymbol{\omega}$ is the wing's angular velocity. In this case, assuming a perfectly horizontal stroke plane ($\psi = 0$, $\dot{\psi} = 0$), it follows that $\boldsymbol{\omega} = \dot{\phi}\hat{\mathbf{Z}} + \dot{\theta}\hat{\mathbf{y}}$, where θ is the only generalized coordinate of the system and $\{\phi, \dot{\phi}\}$ are fully prescribed, as flapping motions are actively generated, as shown in Fig. 1-(c). Thus, the equation of motion associated with the generalized coordinate θ completely describes the dynamical behavior of the system according to

$$J_y\ddot{\theta} = M_{\mathrm{ae},\mathbf{y}} - k_\mathrm{h}\theta - J_{yz}\ddot{\phi}\cos\theta + \frac{1}{2}J_y\dot{\phi}^2\sin 2\theta, \qquad (2)$$

where J_y and J_{xy} are the wing's moment of inertia components in the body frame $\mathbb{F}_\mathrm{b}$, $M_{\mathrm{ae},\mathbf{y}}$ is the component of the

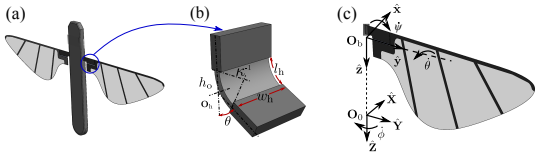

Fig. 1. Robotic flapping-wing system. (a) Illustration of the generic flapping-wing microrobot considered in this research. (b) Geometric model of the flexure hinge mechanism. (c) Definition of the coordinate systems. The inertial frame $\mathbb{F}_0$ is defined by the fixed origin $\mathbf{O}_0$ and space-fixed unit vectors $\hat{\mathbf{X}}$, $\hat{\mathbf{Y}}$, $\hat{\mathbf{Z}}$. The body frame $\mathbb{F}_\mathrm{b}$ is defined by the origin $\mathbf{O}_\mathrm{b}$ and instantaneous wing-fixed unit vectors $\hat{\mathbf{x}}$, $\hat{\mathbf{y}}$, $\hat{\mathbf{z}}$. The Euler angles ϕ, θ, ψ denote the flapping, pitching and rolling rotations of the wing, respectively.

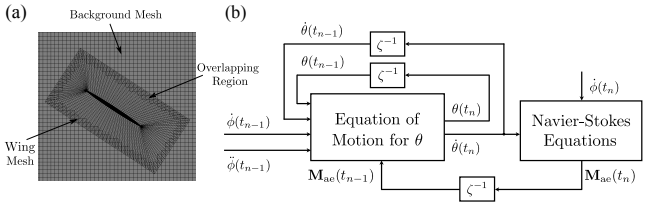

Fig. 2. Overset grid and data-flow diagram. (a) Example of overset grid assembly for a rotating wing. (b) Diagram of the integrated simulation procedure. Here, t_n is discrete time, $\mathbf{M}_\mathrm{ae}$ is the integrated aerodynamic moment on the wing surface, and ζ^{-1} is the unit delay operator.

This extended abstract presents results published in the Proceedings of the AIAA Atmospheric Flight Mechanics Conference, AIAA SciTech (AIAA 2016-0013), January 2016. This work was supported by the USC Viterbi School of Engineering through a graduate fellowship to L. Chang and a start-up fund to N. O. Pérez-Arancibia.

The authors are with the Department of Aerospace and Mechanical Engineering, Viterbi School of Engineering, University of Southern California (USC), Los Angeles, CA 90089, USA (email: longlonc@usc.edu; perezara@usc.edu).

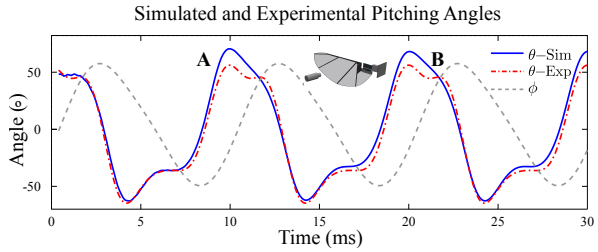

Fig. 3. Passive-pitching simulation results. Comparison between the simulated wing-pitching angle, θ-Sim, and the experimentally measured wing-pitching angle in [2], θ-Exp. The wings in the simulation and experiment are driven according to the same prescribed flapping signal ϕ (gray dashed line). A simplified illustration of the experiment in [2] is shown between markers A and B.

aerodynamic moment $\mathbf{M}_{\text{ae}}$ along the axis $\hat{\mathbf{y}}$, as defined in Fig. 1-(c), and k_{h} is the spring constant of the hinge.

III. Simulation and Validation

The continuum air flows around the wings of the aerial microrobots considered here, which operate at low Reynolds numbers, are 3-D, unsteady and describable by the 3-D incompressible Navier-Stokes equations, as

$$\begin{aligned} \nabla \cdot \mathbf{u} &= 0 \\ \frac{\partial \mathbf{u}}{\partial t} + \mathbf{u} \cdot \nabla \mathbf{u} &= -\frac{1}{\rho} \nabla p + \nu \nabla^2 \mathbf{u}, \end{aligned} \tag{3}$$

where $\mathbf{u}$ is the flow velocity field, p is the air pressure field, ρ is the air density and ν is the air kinematic viscosity. In the simulations presented in this abstract, (3) is solved numerically, using a finite-volume-based implicit unsteady segregated solver, available with the STAR-CCM+ package. As illustrated in Fig. 1, since a robot's wing moves during the simulation process, the overset grid method shown in Fig. 2-(a) is used to update the instantaneous global mesh for the 3-D aerodynamic solver in a way such that all the local mesh domains are assembled together dynamically.

As shown in the scheme of Fig. 2-(b), the Navier-Stokes equations are solved in a discretized space, the spatial distributions of pressure and velocity are computed, and the aerodynamic moment, M_{ae}, is obtained by integrating the pressure and sheer-stress contributions over the boundary surface of the wing. The dynamics of the wing, i.e., (1), are solved using an alternating time marching procedure in which the solution to the rigid-body dynamics of the wing at time t_n is updated using the total aerodynamic moment at t_{n-1}. Then, the updated rigid-body wing dynamics information is employed to find the boundary conditions required to solve the Navier-Stokes equations at time t_n. The numerical solvers employed to solve the equation of motion (1) and the Navier-Stokes equations (3) are combined to generate the simulation scheme in Fig. 2-(b).

In the course of the research discussed here, the proposed integrated simulation approach has been validated by comparing the computed pitching angles with the experimental data published in [2]. In the implementation of the simulations we use the experimental flapping signal ϕ in Fig. 3 (taken from [2]), obtained experimentally, in open loop, by exciting the microrobotic mechanism's actuator with a sinusoidal function. Notice that since ϕ in Fig. 3 is generated experimentally and in open loop, this signal is not perfectly sinusoidal. As can be seen in Fig. 3, the simulated pitching angle signal, θ-Sim, matches reasonably well the experimental signal, θ-Exp, with the exception of the signal peaks (marked with A and B), which provides

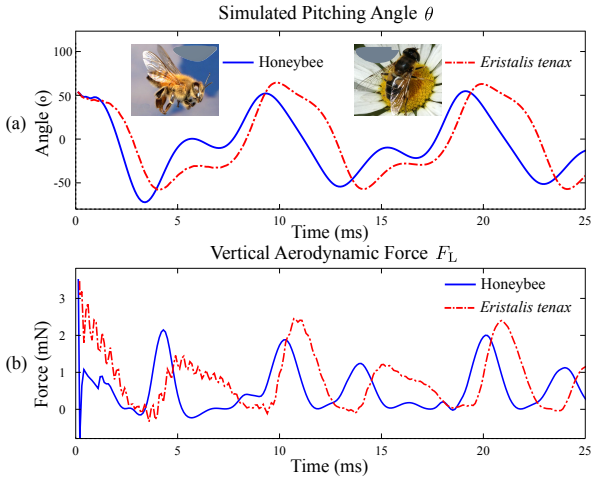

Fig. 4. Comparison of passive-pitching simulation results obtained with the models of a rigid honeybee-like wing and a rigid *Eristalis tenax*-like wing for a stiffness $k_{\text{h}} = 3\ \mu\text{mN} \cdot \text{rad}^{-1}$. (a) Simulated pitching-angle signals comparing the honeybee-like wing and *Eristalis tenax*-like wing cases. (b) Simulated instantaneous total vertical aerodynamic forces corresponding to the honeybee-like-wing and *Eristalis tenax*-like wing cases.

evidence supporting the effectiveness of the proposed integrated simulation approach. The observed discrepancies at the peaks A and B in Fig. 3 suggest that the assumptions of a perfectly rigid wing and a spring-like hinge might not be completely correct. This issue is a matter of current and further research.

IV. Applications

The proposed integrated simulation approach, illustrated by the data-flow diagram in Fig. 2-(b), can be employed to investigate a number of research topics relevant to the understanding of flapping-wing microrobots. For example, the instantaneous location of the center of pressure, energy consumption, the effects of the flexure hinge stiffness on the dynamical behavior of the system and the influence of the wing planform shape on the robot's performance.

The simulation results for two different wing planform shapes are shown in Fig. 4. The first planform shape corresponds to a honeybee-like wing and the second planform shape corresponds to a *Eristalis tenax*-like wing. For comparison purposes, in the implementation of the simulations, the planform shapes of the two wings are re-shaped so that both simulated wings have very similar spanwise lengths and surface areas. Also, both wings are designed so that they define identical moments of inertia with respect to their principal axes. The main difference between the two simulated wings is that the honeybee-like wing has a sharper trailing edge than that of the *Eristalis tenax*-like wing. From the comparison in Fig. 4, it can be observed that the signals corresponding to the honeybee-like wing display a significant phase shift and that the *Eristalis tenax*-like wing produces larger instantaneous and average vertical forces, which suggests that the planform shape can significantly affect the aerodynamic efficiency of micro-flyers propelled by passively-pitching flapping wings.

References

[1] R. J. Wood, "The First Takeoff of a Biologically Inspired At-Scale Robotic Insect," *IEEE Trans. Robot.*, vol. 24, no. 2, pp. 341–347, Apr. 2008.

[2] J. P. Whitney and R. J. Wood, "Aeromechanics of passive rotation in flapping flight," *J. Fluid Mech.*, vol. 660, pp. 197–220, Oct. 2010.

[3] B. Liang and M. Sun, "Nonlinear flight dynamics and stability of hovering model insects," *J. R. Soc. Interface*, vol. 10, no. 85, p. 20130269, 2013.